J. Fluid Mech. (2021), *vol.* 914, F1, doi:10.1017/jfm.2020.1079

JFM FOCUS ON FLUIDS

Special JFM volume in celebration of the George K. Batchelor centenary

Extreme events in turbulent flow

H.K. Moffatt†

Department of Applied Mathematics and Theoretical Physics, University of Cambridge, Wilberforce Road, Cambridge CB3 0WA, UK

(Received 31 October 2020; accepted 31 October 2020)

Extreme events in turbulent flow are associated with intense stretching of concentrated vortices, intermittent in both space and time. The occurrence of such events has been investigated in a turbulent flow driven by counter-rotating propellors (Debue *et al.*, *J. Fluid Mech.*, 2021), and local flow structures have been identified. Interesting theoretical problems arise in relation to this work; these are briefly considered in this focus paper.

Key words: intermittency, topological fluid dynamics, vortex dynamics

1. Introduction

A central challenge in the theory of turbulence is to resolve the precise mechanism by which energy is dissipated in the limit of very high Reynolds number $Re \gg 1$. In homogeneous turbulence, the mean rate of dissipation of energy ϵ is given by $\epsilon = \nu \left\langle \boldsymbol{\omega}^2 \right\rangle$. Here, ν is the kinematic viscosity of the fluid, $\boldsymbol{\omega}(\boldsymbol{x}, t) = \boldsymbol{\nabla} \times \boldsymbol{u}(\boldsymbol{x}, t)$ is the vorticity field, $\boldsymbol{u}$ is the velocity field and the angular brackets $\langle \cdots \rangle$ denote a space average. In the widely accepted, although simplistic, scenario of Kolmogorov (1941), the turbulence acquires its mean kinetic energy $\left\langle \boldsymbol{u}^2 \right\rangle /2 = u_0^2/2$ on a scale ℓ_0 at a rate $\epsilon \sim u_0^3/\ell_0$; this energy cascades down through the 'inertial range' of scales to the Kolmogorov scale $\ell_\nu \sim (\epsilon/\nu^3)^{1/4} \sim Re^{-3/4}\ell_0$, below which it is dissipated by viscosity. On dimensional grounds, the all-important parameter ϵ determines the energy spectrum $E(k) = C\epsilon^{2/3}k^{-5/3}$ in the inertial range, where C is supposedly a universal constant and k is the wavenumber. The vorticity spectrum $k^2E(k)$ thus rises like $k^{1/3}$ through the inertial range, peaking at a wavenumber k of order $k_\nu = \ell_\nu^{-1}$, consistent with $\left\langle \boldsymbol{\omega}^2 \right\rangle \sim \epsilon/\nu$. The fundamental process of vortex stretching is responsible for the cumulative intensification of vorticity on ever-decreasing length scales.

Following Kolmogorov (1962), it has been known for some time from direct numerical simulations that this process of vorticity intensification is extremely intermittent (see, for example, Ishihara *et al.* 2007). With decreasing scale, the vorticity distribution becomes more and more concentrated in singular structures that look like highly distorted sheets or filaments of vorticity. The sheets have a natural tendency to break up into filaments

† Email address for correspondence: hkm2@damtp.cam.ac.uk

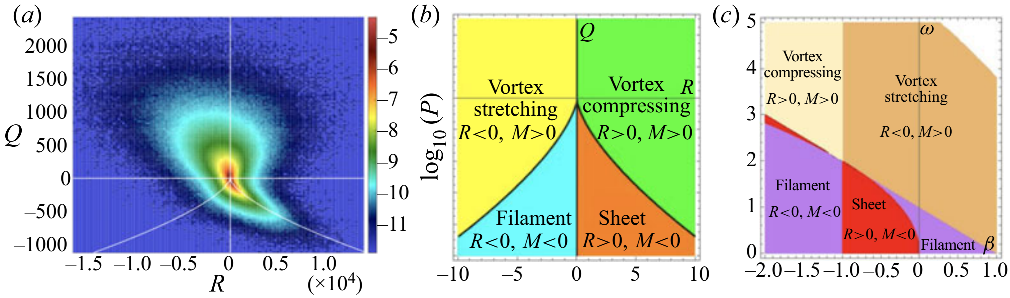

Figure 1. (a) Reproduction of figure 4(a) from DVC showing the joint p.d.f. (probability density function) of R and Q, with dark red representing the maximum probability; the tear-drop region is the location where most extreme events are found, as shown in their figure 5(a) (not shown here); (b) the four regions of the same plane in which topologically distinct structures, as indicated, were identified; the cusped curve is $M(R, Q) \equiv 27R^2 + 4Q^3 = 0$; ($c$) corresponding divisions of the $\{\beta, \omega_0\}$ plane, when the local velocity field takes the idealised form $\boldsymbol{u} = (-\alpha x - (\omega_0 y)/2, -\beta y + (\omega_0 x)/2, (\alpha + \beta)z)$ (with $\alpha = 1$), as on the axis of a Burgers-type vortex.

by elliptic and/or Kelvin–Helmholtz instabilities (McKeown *et al.* 2018). Such vortex filaments were first detected experimentally by Douady, Couder & Brachet (1991), intermittent in both space and time (see also Rusaouën, Rousset & Roche (2017) for similar observations in liquid helium).

2. Most extreme events of local energy transfer

An important advance has now been made in the detection of near-singular structures in a turbulent flow that is driven by counter-rotating propellors in the ‘von Kármán’ configuration (Debue *et al.* 2021; hereafter DVC). These propellors drive a mean flow with a non-zero helicity that is presumably inherited by the turbulence. By the use of tomographic particle velocimetry, the authors have identified ‘extreme events of local energy transfer’, and have determined the structure of the local velocity and vorticity fields in each case. The Reynolds number based on the propellor geometry and rotation rate varied over the range 6.3×10^3 to 3.1×10^5; at the lower end of this range, it was possible to resolve structures on the dissipative length scale $\ell_\nu \sim 1.4$ mm, whereas at the upper end only the inertial range was accessible.

Classification of extreme events has been based by DVC on the non-zero invariants of the velocity-gradient tensor $S_{ij} = \partial u_i/\partial x_j$, defined by $Q(\boldsymbol{x}) = -(S_{ij}S_{ji})/2$, $R(\boldsymbol{x}) = -\det[S_{ij}]$. If $M(R, Q) \equiv 27R^2 + 4Q^3 < 0$, the three eigenvalues of S_{ij} are real, and local irrotational strain dominates over vorticity. If $M > 0$, one eigenvalue is real and the other two are complex conjugates, so vorticity dominates and streamlines are locally spiral or helical in character. Figure 1(a) reproduces figure 4(a) from DVC: in this, the tear-drop region shows where, in the $\{R, Q\}$ plane, most extreme events are found (see also their figure 5(a), not shown here). Figure 1(b) shows the basic structure of this figure, in which this plane is separated into four regions in which topologically distinct structures were identified: vortex stretching; vortex compressing; sheets; and filaments.

DVC found that the most extreme events of local energy transfer occurred in the vortex-stretching and vortex-compressing regions. It may be helpful to interpret this finding with reference to a simple vortical flow of the form

$$\boldsymbol{u}_v(\boldsymbol{x}) = \frac{\omega_0}{2\, r^2}(1 - \mathrm{e}^{-r^2})(-y, x, 0), \quad \boldsymbol{\omega} = \nabla \times \boldsymbol{u}_v(\boldsymbol{x}) = (0, 0, \omega_0\, \mathrm{e}^{-r^2}), \qquad (2.1a,b)$$

https://doi.org/10.1017/jfm.2020.1079 Published online by Cambridge University Press

where $r^2 = x^2 + y^2$, this vortex being stretched by the non-axisymmetric strain field

$$\boldsymbol{U} = (-\alpha x, -\beta y, (\alpha + \beta) z), \quad \alpha + \beta > 0. \tag{2.2}$$

At high vortex Reynolds number, such a vortex remains axisymmetric at leading order (Moffatt, Kida & Ohkitani 1994). On the vortex axis $r = 0$, the components of the matrix $\{S_{ij}\}$ are

$$S_{ij} = \begin{pmatrix} -\alpha & -\omega_0/2 & 0 \\ \omega_0/2 & -\beta & 0 \\ 0 & 0 & \alpha + \beta \end{pmatrix}, \tag{2.3}$$

and the corresponding expressions for Q, R and M take the simplified form

$$Q(\alpha, \beta, \omega_0) = -(\alpha^2 + \beta^2 + \alpha\beta) + \omega_0^2/4, \quad R(\alpha, \beta, \omega_0) = -(\alpha + \beta)(\alpha\beta + \omega_0^2/4) \tag{2.4a,b}$$

and

$$M(\alpha, \beta, \omega_0) = 27R^2 + 4Q^3 = -\tfrac{1}{16}[((\alpha - \beta)^2 - \omega_0^2)(8\alpha^2 + 20\alpha\beta + 8\beta^2 + \omega_0^2)]. \tag{2.5}$$

Taking $\alpha = 1$, figure 1(*c*) shows the subdivisions of the $\{\beta, \omega_0\}$ plane corresponding to those of figure 1(*b*). As might be expected, the 'vortex-stretching' region is a sub-region of the half-plane $\alpha + \beta > 0$.

3. Three topological structures – or three in one?

DVC found further that their extreme events were associated with three apparently different topological structures, which they describe as 'screw vortex', 'roll vortex' and 'U-turn'; sample streamlines are shown in their figures 7(*a,b*) and 8(*a*), respectively. They recognise that these structures 'may correspond to a single structure seen at different times or in different frames of reference'. This is an issue that can again be probed through consideration of an explicit vortex-stretching flow. We first replace (2.2) by the modified strain field

$$\boldsymbol{U}_s = (-\alpha x f'(z), -\beta y f'(z), (\alpha + \beta) f(z)), \tag{3.1}$$

with

$$f'(z) = 1 - 2z^2/(1 + z^2), \quad f(z) = -z + 2\tan^{-1} z. \tag{3.2a,b}$$

This flow, which satisfies $\nabla \cdot \boldsymbol{U}_s = 0$, $\nabla \times \boldsymbol{U}_s \neq 0$, could be produced by a system of secondary vortices near the 'primary vortex' (2.1*a,b*). When $\alpha + \beta > 0$, it gives positive stretching for $|z| < 2.33$, negative (i.e. compression) for $|z| > 2.33$. (In this way, vortex stretching may always be coupled with adjacent vortex compression, thus explaining the surprisingly high probability of 'vortex compressing' in the p.d.f. plot of figure 1*a*.) Particle paths (i.e. instantaneous streamlines) of this flow combined with the primary vortex flow (2.1*a,b*) starting from any given point $\boldsymbol{X}(0)$ can be computed from the associated dynamical system $\mathrm{d}\boldsymbol{X}/\mathrm{d}t = \boldsymbol{u}_v(\boldsymbol{X}) + \boldsymbol{U}_s(\boldsymbol{X})$. Their structure depends on the chosen point $\boldsymbol{X}(0)$ and on the frame of reference.

Three examples are shown in figure 2. Here, I have chosen $\alpha = 0.001$, $\beta = 0.0005$, $\omega_0 = 0.2$, so that

$$Q(\alpha, \beta, \omega_0) \approx 0.01, \quad R(\alpha, \beta, \omega_0) \approx -1.5 \times 10^{-5}, \quad M(\alpha, \beta, \omega_0) \approx 4 \times 10^{-6}, \tag{3.3a–c}$$

and (for $|z| < 2.33$) we are indeed in the vortex-stretching regime $R < 0$, $M > 0$. Although computed from the same velocity field in the same vortex neighbourhood, these streamline

https://doi.org/10.1017/jfm.2020.1079 Published online by Cambridge University Press

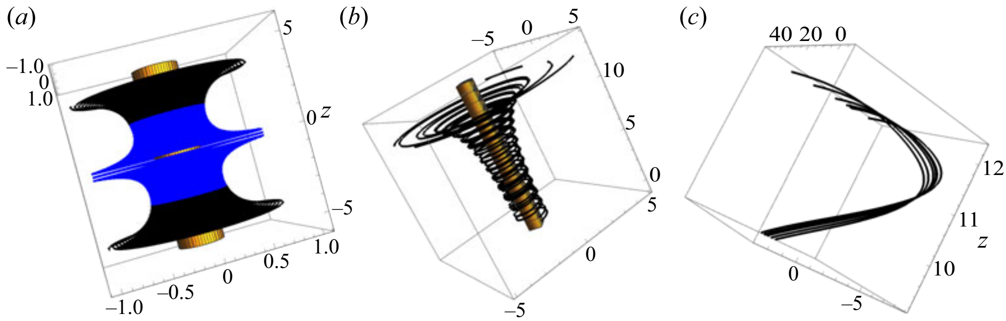

Figure 2. Streamlines computed from the dynamical system $\mathrm{d}\boldsymbol{X}/\mathrm{d}t = \boldsymbol{u}_v(\boldsymbol{x}) + \boldsymbol{U}_s(\boldsymbol{x})$; $\alpha = 0.001$, $\beta = 0.0005$, $\omega_0 = 0.2$; the vorticity contour $\omega/\omega_0 = 0.3$ is shown in brown, and, as in DVC, streamlines are shown in blue when approaching the vortex, black when leaving it; (*a*) $\boldsymbol{X}(0) = (1, 0, \pm 0.01)$ and $(1, 0, \pm 0.2)$; (*b*) the same streamlines viewed in a frame of reference moving with velocity $(0, 0, -0.01)$; $\boldsymbol{X}(0) = (1, 0, \pm 0.2)$; (*c*) eight streamlines starting from points close to $\boldsymbol{X}(0) = (2.87, 0, 0)$ and plotted for dimensionless time $1000 \le t \le 4000$ when they first 'encounter' the vortex.

patterns nevertheless look quite different: figures 2(*a*), 2(*b*) and 2(*c*) have structures comparable with those of DVC's screw vortex, roll vortex and U-turn, respectively. Thus care is certainly needed in classifying such observed structures, for which vorticity is presumably a more robust topological feature than velocity.

Declaration of interest. The author reports no conflict of interest.

Author ORCIDs.
H.K. Moffatt https://orcid.org/0000-0003-2575-5111.

References

Debue, P., Valori, V., Cuvier, C., Daviaud, F., Foucaut, J.-M., Laval, J.-P., Wiertel, C., Padilla, V. & Dubrulle, B. 2021 3D analysis of precursors to non-viscous dissipation in an experimental turbulent flow. *J. Fluid Mech.*

Douady, S., Couder, Y. & Brachet, M.E. 1991 Direct observation of the intermittency of intense vorticity filaments in turbulence. *Phys. Rev. Lett.* **67**, 983–986.

Ishihara, T., Kaneda, Y., Yokokawa, M., Itakura, K. & Uno, A. 2007 Small-scale statistics in high-resolution direct numerical simulation of turbulence: Reynolds number dependence of one-point velocity gradient statistics. *J. Fluid Mech.* **592**, 335–366.

Kolmogorov, A.N. 1941 The local structure of turbulence in incompressible viscous fluid for very large Reynolds numbers. *Dokl. Akad. Nauk SSSR* **30**, 299–303.

Kolmogorov, A.N. 1962 A refinement of previous hypotheses concerning the local structure of turbulence in a viscous incompressible fluid at high Reynolds number. *J. Fluid Mech.* **13**, 82–85.

McKeown, R., Ostilla-Monico, R., Pumir, A., Brenner, M.P. & Rubinstein, S.M. 2018 A cascade leading to the emergence of small structures in vortex ring collisions. *Phys. Rev. Fluids* **3**, 124702.

Moffatt, H.K., Kida, S. & Ohkitani, K. 1994 Stretched vortices – the sinews of turbulence; large-Reynolds-number asymptotics. *J. Fluid Mech.* **259**, 241–264 and **266**, 371.

Rusaouën, E., Rousset, B. & Roche, P.-E. 2017 Detection of vortex coherent structures in superfluid turbulence. *Europhys. Lett.* **118** (1), 14005.

https://doi.org/10.1017/jfm.2020.1079 Published online by Cambridge University Press